UC Irvine

UC Irvine Previously Published Works

Title

Causal Evidence that Rotational Moisture Advection is Critical to the Superparameterized Madden-Julian Oscillation

Permalink

https://escholarship.org/uc/item/17f5b45q

Journal

Journal of the Atmospheric Sciences, 71(2)

ISSN

0022-4928 1520-0469

Authors

Pritchard, Michael S
Bretherton, Christopher S

Publication Date

2014-02-01

DOI

10.1175/JAS-D-13-0119.1

Copyright Information

This work is made available under the terms of a Creative Commons Attribution License, availalbe at https://creativecommons.org/licenses/by/4.0/

Peer reviewed

eScholarship.org Powered by the California Digital Library
University of California

Causal Evidence that Rotational Moisture Advection is Critical to the Superparameterized Madden–Julian Oscillation

MICHAEL S. PRITCHARD AND CHRISTOPHER S. BRETHERTON

University of Washington, Seattle, Washington

(Manuscript received 22 April 2013, in final form 27 August 2013)

ABSTRACT

The authors investigate the hypothesis that horizontal moisture advection is critical to the eastward propagation of the Madden–Julian oscillation (MJO). Consistent diagnostic evidence has been found in recent MJO-permitting global models viewed from the moisture-mode dynamical paradigm. To test this idea in a causal sense, tropical moisture advection by vorticity anomalies is artificially modulated in a superparameterized global model known to produce a realistic MJO signal. Boosting horizontal moisture advection by tropical vorticity anomalies accelerates and amplifies the simulated MJO in tandem with reduced environmental gross moist stability. Limiting rotational horizontal moisture advection shuts the MJO down. These sensitivities are robust in that they are nearly monotonic with respect to the control parameter and emerge despite basic-state sensitivities favoring the opposite response. Speedup confirms what several diagnostic lines of evidence already suggest—that anomalous moisture advection is fundamental to MJO propagation. The rotational component is shown to be especially critical. Amplification further suggests it may play a role in adiabatically maintaining the MJO.

1. Introduction

The Madden–Julian oscillation (MJO) has been hypothesized to be a ''moisture mode.'' Moisture is especially fundamental to the dynamics of tropical convective disturbances because equatorial scalings of the primitive equations include latent heating active at leading order and weak temperature gradient balance (Sobel et al. 2001). Energetic thermodynamic feedbacks can thus occur between moisture anomalies and their effect through deep convection on circulations, evaporative fluxes, and radiative heating (Raymond et al. 2009; Sobel and Maloney 2012). On long time scales, such feedbacks enable an intrinsic predisposition for deep convection to self-organize on very large scales in undisturbed radiative convective equilibrium (Bretherton et al. 2005; Muller and Held 2012). On short time scales, similar thermodynamic feedbacks are relevant to the physics of transient tropical convective disturbances. This is the general moisture-mode dynamical paradigm (Raymond et al. 2009). Sobel and Maloney (2012) provide a good definition of what it means to view the MJO as a moisture mode.

A rich variety of idealized moisture-mode dynamics have been identified and analyzed in reduced-order mathematical models of tropical disturbances (Yu and Neelin 1994; Fuchs and Raymond 2002, 2005; Sugiyama 2009a,b; Raymond and Fuchs 2009; Sobel and Maloney 2013). While dynamically insightful, low-order models have limitations for understanding the Madden–Julian oscillation, which is inextricable from a broad spectrum of nonlinear diabatic and dynamical feedback processes. Observational analysis and high degree of freedom global atmospheric modeling are thus especially attractive tools for understanding MJO physics.

Recent experience with reanalyses and global numerical models has proved consistent with a moisture-mode paradigm and suggests an especially critical role for horizontal moisture advection in controlling the eastward propagation of the MJO. Tightening the parameterized coupling of column humidity and deep convection—a cornerstone of analytic moisture-mode theory—improves the MJO signal in several weather and climate models (Maloney 2009; Maloney et al. 2010; Hannah and Maloney 2011; Hirons et al. 2013; Chikira and Sugiyama 2013). In both reanalyses and MJO-permitting models,

Corresponding author address: Michael S. Pritchard, 408 Atmospheric Sciences Geophysics (ATG) Building, Box 351640, Seattle, WA 98195-1640.
E-mail: mspritch@uw.edu

DOI: 10.1175/JAS-D-13-0119.1

© 2014 American Meteorological Society

composites of MJO-related fluctuations of column moist static energy (MSE) balance terms reveal zonal phase quadrature patterns suggesting that horizontal moisture advection is central to MJO propagation (Benedict and Randall 2007; Maloney 2009; Maloney et al. 2010; Kiranmayi and Maloney 2011; Andersen and Kuang 2012; Chikira 2014).

The above diagnostic relationships from global models and reanalyses motivate the hypothesis that horizontal moisture advection is critical to MJO propagation. But they are not sufficient to prove it in a causative sense. For this, mechanism interference simulation experiments are helpful. Examples of such work already exist in the form of binary aquaplanet simulation pairs with perturbed basic-state SSTs. For instance, Maloney et al. (2010) sharpened the investigation into the importance of zonal moisture advection by weakening the zonal SST gradient in their model, which resulted in a weaker background westerly flow and slower MJO propagation speed. Others have recently found that narrowing the meridional moisture gradient or tripling anomalous horizontal moisture advection on a zonally symmetric aquaplanet can result in systematic MJO speedup (Anderson 2012).

This paper expands on the investigation of whether a clean causal link between MJO phase speed and moisture advection can be demonstrated in a global model with a realistic MJO. This is achieved by analyzing the sensitivity of the superparameterized MJO to surgically interfering with horizontal moisture advection by vorticity anomalies in the tropics. Two novel elements of our experiment design compared to the above work are 1) that it focuses on just the role of the rotational component of the moisture advection and 2) that it focuses on a version of the Superparameterized Community Atmosphere Model (SPCAM) that has a well-validated MJO signal and a realistic (real geography) basic state. The first point is inspired by a philosophical view that vorticity is one of the likely sources of memory available in the tropics to help explain the slowness of the MJO as an internal atmospheric disturbance. The second point aims to break tradition with the practice of examining the role of moisture advection in models with highly idealized basic states or with restricted feedbacks. It is complementary to examine the advection process and its influence on the MJO in its native state with real geography and full nonlinear coupling to a range of diabatic feedbacks.

Sections 2 and 3 describe the modeling setup and advection interference strategy. Section 4 describes the resulting MJO and basic-state response. Key sensitivities of the MJO and high-frequency tropical wave modes are discussed in section 5 and conclusions summarized in section 6.

2. Model description

The baseline code used for all simulations is the prototype version of SPCAM, version 3.0, as archived [https://svn.sdsc.edu/repo/cmmap/cam3_sp (rev. 80)] by the Center for Multiscale Modeling of Atmospheric Processes. The global scale is represented by a version of CAM that slightly predates the CAM3.0 release. Global dynamics are formulated spectrally, with a semi-Lagrangian advection scheme, on 30 vertical levels. Horizontal resolution is truncated at T42. The interior 2D cloud system–resolving scale is represented using the System for Atmospheric Modeling described in Khairoutdinov and Randall (2003), which replaces conventional cloud and boundary layer parameterizations in CAM.

This old, established version of SPCAM is chosen for analysis because it is known to produce a free-running MJO and mean–boreal winter tropical climatology that compare favorably with observations when run with prescribed sea surface temperatures (Randall et al. 2003; Khairoutdinov et al. 2005, 2008; Benedict and Randall 2009; Thayer-Calder and Randall 2009). In contrast, newer versions of SPCAM produce an eroded mean-state climatology and degraded MJO signals under similar boundary forcing (not shown). This is likely not an intrinsic sensitivity of superparameterization but may be a reflection of the fact that new versions of SPCAM are rapidly evolving and have not been substantially tuned[1] since version 3.0.

We have chosen to use the uncoupled version for simplicity but acknowledge that it is a limitation of this study. When SPCAM3.0 is instead coupled to a slab ocean model (Benedict and Randall 2011) or fully dynamic ocean model (Stan et al. 2010) it produces even more realistic MJO structures, particularly over the western and central Pacific, where surface flux feedbacks in the uncoupled model are overly vigorous (Benedict and Randall 2009) and the Kelvin wave component of the composite signal is underrepresented (Benedict and Randall 2011).

To speed up calculations in this study, SPCAM's embedded cloud arrays are reduced to a quarter of their typical 128-km extent. That is, only eight columns are used per CRM array, spanning 32 km in the north–south direction. This CRM configuration was previously explored in Khairoutdinov et al. (2005), who reported that it did not significantly alter the mean climate in SPCAM3.0. In short-duration simulations, they also

[1] The tropical mean TOA radiation in SPCAM3.0 is remarkably realistic, owing to judicious tuning of unconstrained CRM microphysics parameters (M. Khairoutdinov 2012, personal communication). This time-consuming process has not been repeated for newer versions of SPCAM.

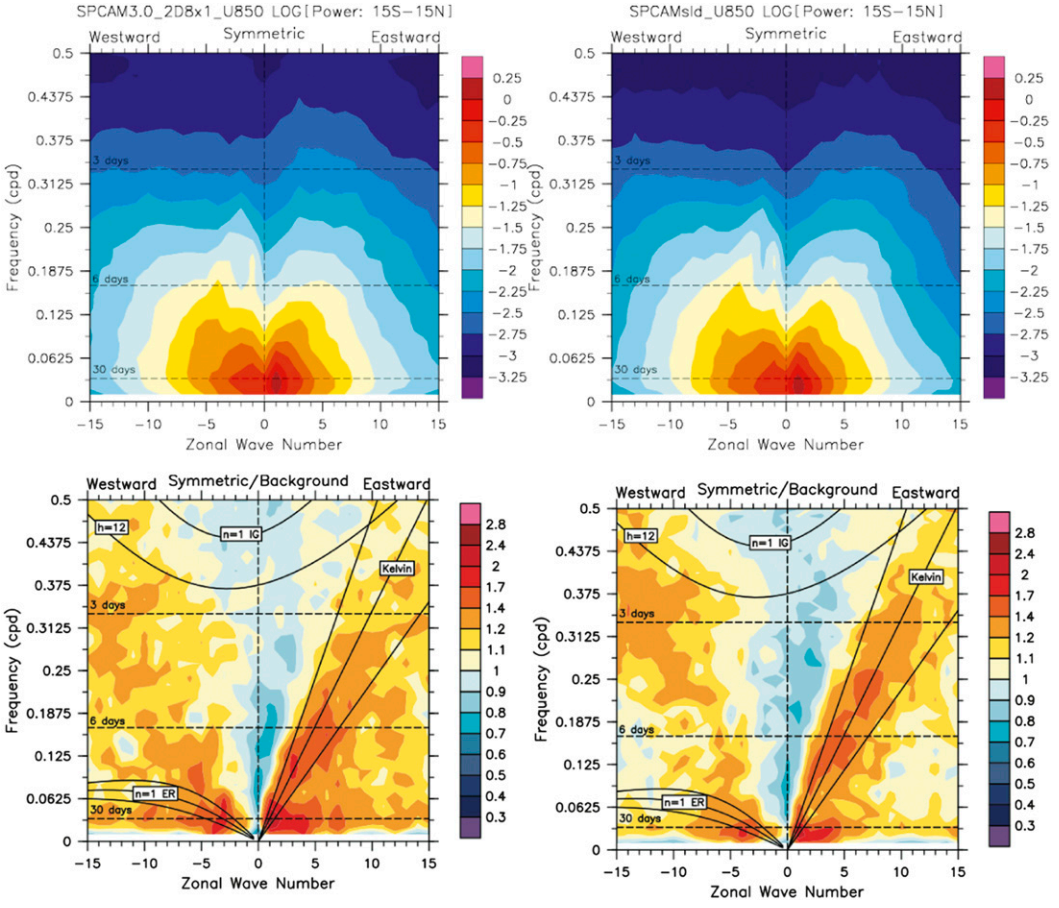

FIG. 1. Wavenumber–frequency (top) U850 spectra and (bottom) OLR signal-to-noise spectra for 15°S–15°N anomalies from the mean annual cycle from 8-yr control SPCAM runs, for the case of using (left) unusually small cloud-resolving model (CRM) arrays of 32 km in extent, as in this study, vs (right) the typical configuration of 128-km extent.

noticed comparable intraseasonal variability using the smaller CRM configuration (D. Randall 2012, personal communication). We have confirmed in long runs that SPCAM's simulated MJO is indeed robust to this reconfiguration and in general to many details of its mesoscale organization. Figure 1 demonstrates the robustness of the simulated equatorial wave spectrum as justification for the decision to use small CRMs.

All simulations are run for 7 years (1980–86) with surface boundary forcing prescribed from time-varying monthly mean observed sea surface temperatures. In addition to a control experiment, eight tests with perturbed advection are conducted as described below.

3. Modulating rotational moisture advection

A control parameter is implemented in SPCAM to isolate the sensitivity of its MJO to anomalous rotational moisture advection.

In SPCAM's host semi-Lagrangian dynamical core, spectral horizontal velocity coefficients are calculated following the solution to a vorticity equation as linear combinations of divergence (δ) and vorticity (ζ) spectral coefficients. That is,

$$\mathbf{u}^{m,n} = a^{m,n}\delta^{m,n} + b^{m,n}(\zeta^{m,n} + f), \qquad (1)$$

where the superscripts m and n denote the order and rank of a Legendre mode, f is planetary vorticity, and the formulation of $a^{m,n}$ and $b^{m,n}$ for each component of horizontal velocity can be found in Eqs. (3.186)–(3.187) of Collins and Rasch (2004).

We calculate an auxiliary velocity represented spectrally by $\tilde{\mathbf{u}}^{m,n}$, whose contribution from anomalous vorticity is modulated by the control parameter α,

$$\tilde{\mathbf{u}}^{m,n} = a^{m,n}\delta^{m,n} + b^{m,n}[\zeta_0^{m,n} + \alpha(\zeta^{m,n} - \zeta_0^{m,n}) + f], \qquad (2)$$

where ζ_0 is a daily mean climatological annual cycle of three-dimensional spectral vorticity, accumulated offline from the control simulation and linearly interpolated to the model's internal calendar day.

To limit effects of α to the equatorial zone, after synthesis of the full velocities $\mathbf{U}$ and $\tilde{\mathbf{U}}$ from their spherical harmonic subcomponents on the global Gaussian grid, the hybrid auxiliary velocity $\widetilde{\mathbf{U}_h}$ is calculated as

$$\widetilde{\mathbf{U}_h} = \begin{cases} \dfrac{(\mathbf{U}-\tilde{\mathbf{U}})}{1+e^{-2k(\phi-\phi_0)}} + \tilde{\mathbf{U}} & \text{if} \quad \phi \geq 0 \\ \dfrac{(\mathbf{U}-\tilde{\mathbf{U}})}{1-e^{-2k(\phi-\phi_0)}} + \tilde{\mathbf{U}} & \text{if} \quad \phi < 0 \end{cases} . \qquad (3)$$

That is, $\widetilde{\mathbf{U}_h}$ transitions smoothly via a smooth Heaviside approximation in latitude ϕ from the vortically perturbed velocity field (equatorward of a critical latitude ϕ_0) to the actual velocity field (poleward of ϕ_0). The parameter values are specified as $k = 0.2$ and $\phi_0 = 20°$.

We interfere with moisture advection by rewiring the input velocities to the semi-Lagrangian advection scheme—for vapor and condensate advection only—such that $\widetilde{\mathbf{U}_h}$ is used in place of $\mathbf{U}$ in calculating Lagrangian trajectories. All other advected variables (e.g., temperature, momentum) are handled with the actual velocity field. The resulting modified SPCAM3.0 code branch that was used to produce all simulations reported in this paper is archived [https://svn.sdsc.edu/repo/cmmap/cam3_sp/branches/pritchard (rev. 304)] at the Center for Multiscale Modeling of Atmospheric Processes.

In summary, an external control parameter has been implemented in SPCAM, whereby $\alpha > 1$ ($0 < \alpha < 1$) amplifies (damps) moisture advection due to tropical ζ anomalies.

4. Results

In addition to a control simulation ($\alpha = 1$) eight 7-yr simulations (1980–86) are analyzed varying α across the values 0.25, 0.5, 0.75, 0.9. 1.1, 1.3, 2.0, and 4.0.

Figure 2 quantifies the magnitude of moisture advection interference for each simulation. For reference, the eight gray curves (one for each of the eight simulations) show the characteristic histogram of the total column MSE tendency due to moisture advection, accumulated across all grid points in 20°S–20°N, from daily mean data spanning the entire 7 years, and independently for each simulation. The corresponding colored lines show adiabatic tendency magnitude histograms accumulated in the same manner but of just the component due to interference by α, color coded by the level of interference in each simulation (i.e., coolest and warmest colors imply the strongest damping and amplification, respectively). By design, the influence of α on gridpoint tendencies of column moist static energy is quantitatively small for values of α close to unity (moderately hued colors; i.e., close to green), but rivals that of the total adiabatic tendency for the most extreme advection interference experiments (warmest and coolest colors; red and blue).

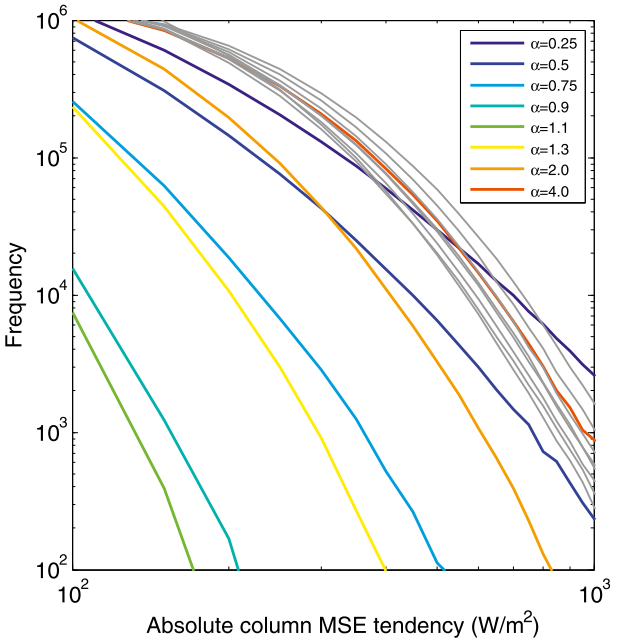

FIG. 2. Histogram of column moist static energy tendencies for 20°S–20°N, showing the magnitude PDF of the total adiabatic tendency (gray) vs the interference component introduced by α (colored) for each simulation.

a. *MJO sensitivity*

The following analysis of SPCAM's MJO makes use of a subset of standard MJO diagnostics established by the Climate Variability and Predictability (CLIVAR) MJO Working Group (Kim et al. 2009).

Figure 3 summarizes the effect of varying α on the amount of wind and cloud variance in the tropics during boreal winter, as computed from daily mean anomalies with respect to a smoothed annual cycle. For $\alpha < 0.5$, SPCAM's convection and wind variance are reduced throughout the tropics, and a smaller fraction of total variance is explained by intraseasonal time scales. This is consistent with a shutdown of the superparameterized MJO when moisture advection by tropical vorticity anomalies is artificially damped. For $\alpha > 1$, total and intraseasonal variances of low-level winds are boosted throughout most of the tropics, which is consistent with an amplification of the MJO when vorticity-induced moisture advection is artificially enhanced. The convective amplitude of the MJO as measured by outgoing longwave radiation (OLR) variance does not scale consistently with the wind amplitude at high α.

Figure 4 displays the geographic footprint of the amplified low-level wind response to increasing α from unity.

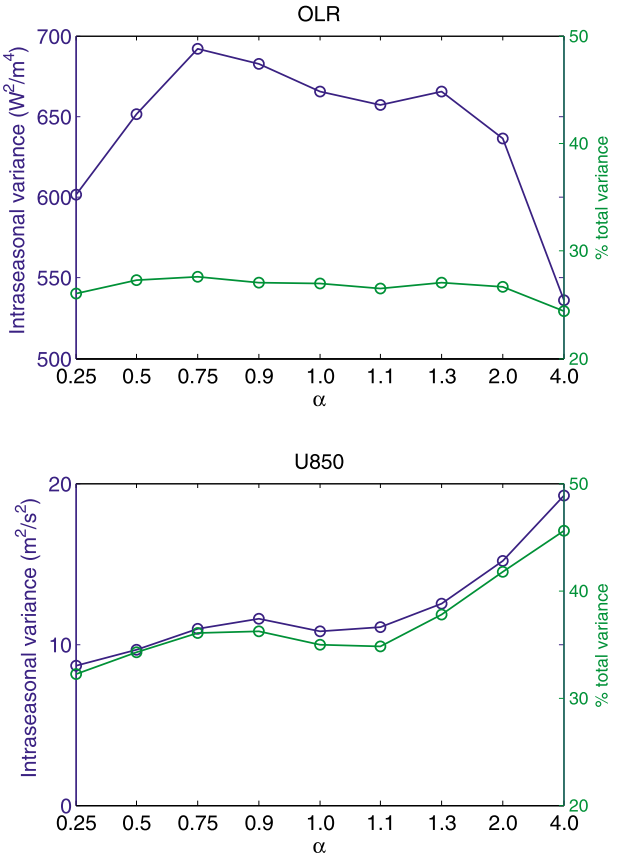

FIG. 3. (top) OLR and (bottom) 850-hPa zonal wind intraseasonal variance (blue) and its percentage of total daily mean variance (green), averaged horizontally from 20°S to 20°N and from 70°E to 110°W, and shown as a function α. The low-level wind variance is amplified at higher α.

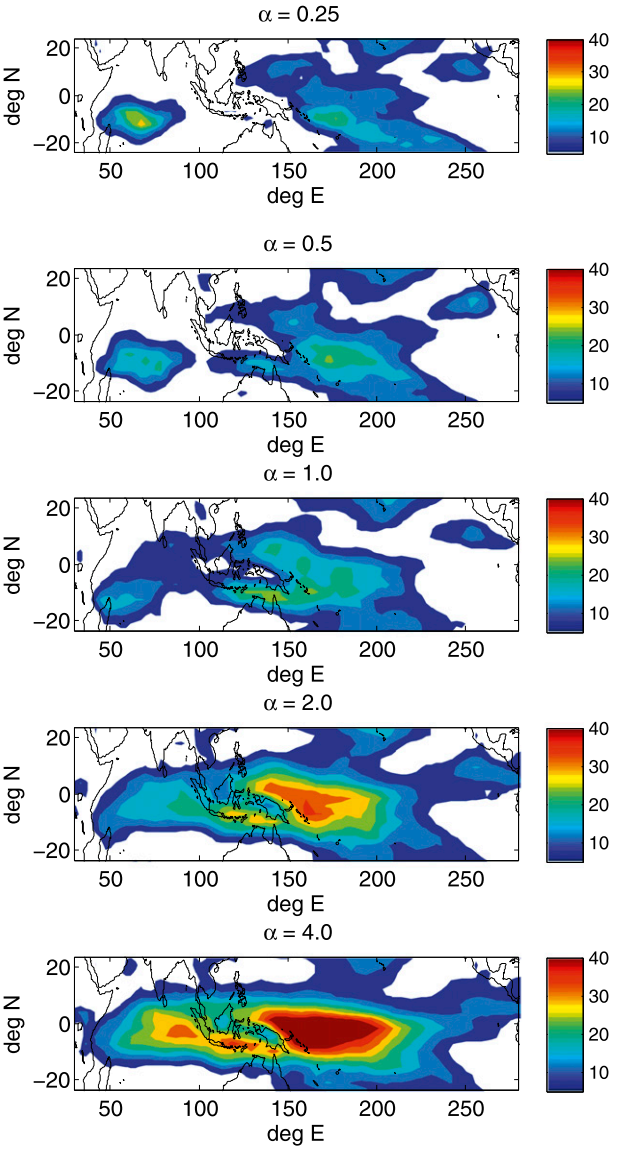

FIG. 4. Maps of the 850-hPa zonal wind anomaly intraseasonal variance ($m^2 s^{-2}$) as a function of (top)–(bottom) increasing α, showing amplification throughout the MJO activity region.

Intraseasonal variance is clearly boosted throughout most of the MJO activity region as α is increased from unity.

Figures 5 and 6 show even clearer evidence of MJO amplification due to increasing α, captured in histograms of the Wheeler–Hendon MJO index (Fig. 5; Wheeler and Hendon 2004) and in the time–longitude statistical structure of the composite boreal winter MJO (Fig. 6). Consistent with the loss in variance, when α is less than unity SPCAM's MJO shuts down as indicated by a shift in the RMM index histogram toward lower values (Fig. 5) and a reduction in the magnitude of the linear correlation between U850 and 20–100-day OLR at 80°E (Fig. 6). Consistent with MJO amplification when α is increased from unity, the high-index tail of the MJO index probability distribution function is boosted (Fig. 5), and the magnitude of the linear correlation between U850 and 20–100-day OLR at 80°E is enhanced (Fig. 6). The spatial phase relationship between OLR and low-level wind anomalies also appears to change somewhat systematically with α.

Interestingly, Fig. 6 also shows that as α is increased from unity SPCAM's simulated MJO speeds up and gains coherence. Figure 7 examines the phase speed change quantitatively. In the control simulation, SPCAM's MJO zonal wind anomalies travel east at approximately $5\,m\,s^{-1}$. As α is increased to 2, the zonal phase speed increases to $6.5\,m\,s^{-1}$. For the extreme case of $\alpha = 4$, an accelerated MJO can be seen to travel at approximately $7.5\,m\,s^{-1}$.

To verify that the effect of α is operating as intended, it is prudent to examine the statistical signatures of eastward traveling column MSE anomalies associated

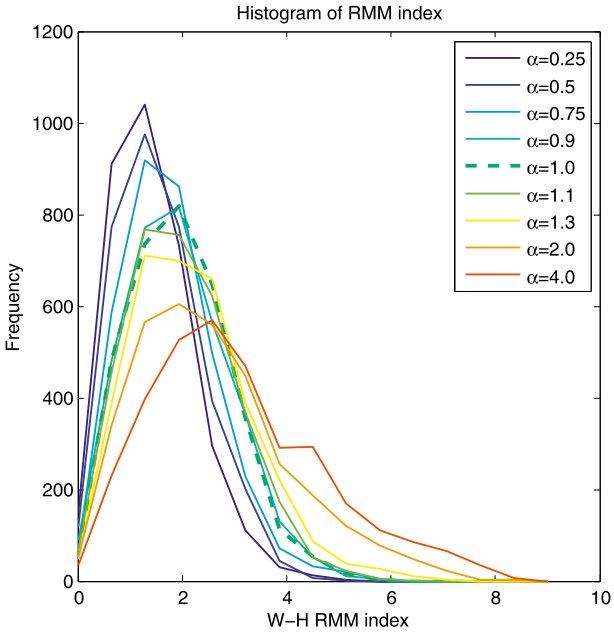

FIG. 5. Histograms of the Wheeler–Hendon RMM index showing MJO amplification as α is increased from unity (warm colors) and the reverse as α is decreased from unity (cool colors). The index is calculated by projecting model anomaly fields onto the leading two observed Wheeler and Hendon multivariate EOFs and taking the square root of the sum of the squares of the leading RMMs (Wheeler and Hendon 2004). The dashed line corresponds to the control simulation with no moisture advection interference.

with SPCAM's MJO. The approximate budget equations governing intraseasonal anomalies of column dry static energy $\langle s \rangle$ and latent energy due to column water vapor $L_v\langle q \rangle$ in our experiments are

$$\left\langle \frac{\partial s}{\partial t} \right\rangle' + \left\langle \mathbf{V} \cdot \nabla s + \omega \frac{\partial s}{\partial p} \right\rangle' \approx \langle \mathrm{LW} \rangle' + L_v P' \quad \text{and} \tag{4}$$

$$\left\langle L_v \frac{\partial q}{\partial t} \right\rangle' + L_v \left\langle \mathbf{V} \cdot \nabla q + \omega \frac{\partial q}{\partial p} \right\rangle' \approx F'_\alpha + \mathrm{LH}' - L_v P', \tag{5}$$

where $\langle \mathrm{LW} \rangle$ is the column-integrated longwave heating rate, L_v is the latent heat of vaporization, LH is the latent heat flux, and P is the precipitation. The first term on the right-hand side of Eq. (5) represents our interference in the moisture budget F_α. All terms are in watts per square meter. The angle brackets denote mass-weighted vertical integration through the depth of the atmospheric column and the primes denote deviations from a climatological mean seasonal cycle containing three seasonal harmonics. The sum of Eqs. (4) and (5) is the column MSE budget equation governing intraseasonal anomalies.

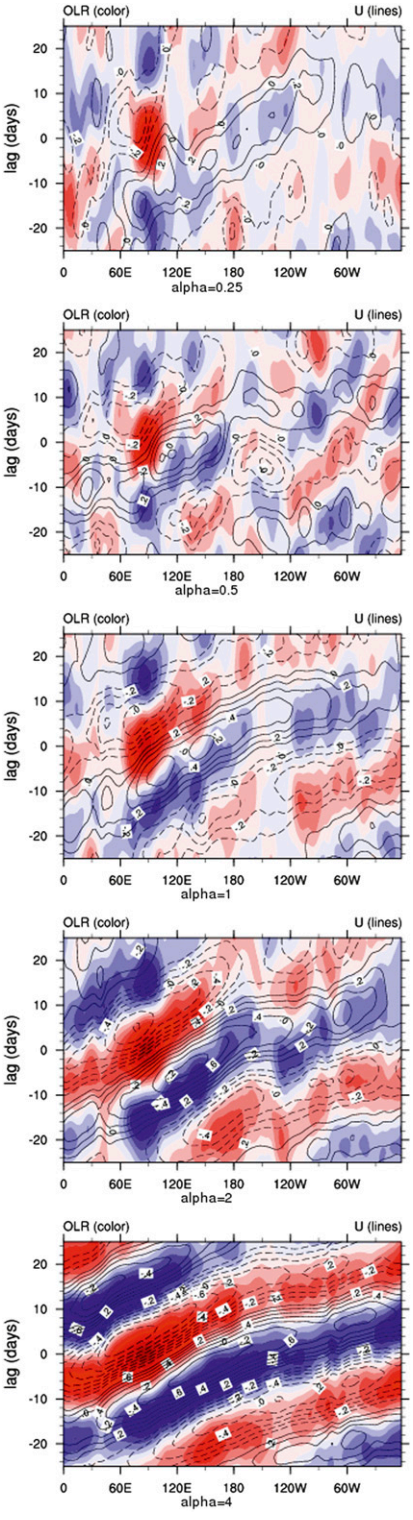

FIG. 6. Time- and longitude-lag correlation coefficients for 15°S–15°N OLR (colors) and zonal wind anomalies (contours) regressed against an MJO-filtered (20–100-day bandpass) OLR time series at 80°E. MJO shutdown is apparent for (top) $\alpha = 0.25$ and (second row) $\alpha = 0.5$. The MJO speeds up and becomes more coherent as α is increased from (third row) unity to (fourth row) $\alpha = 2$ and (bottom) $\alpha = 4$.

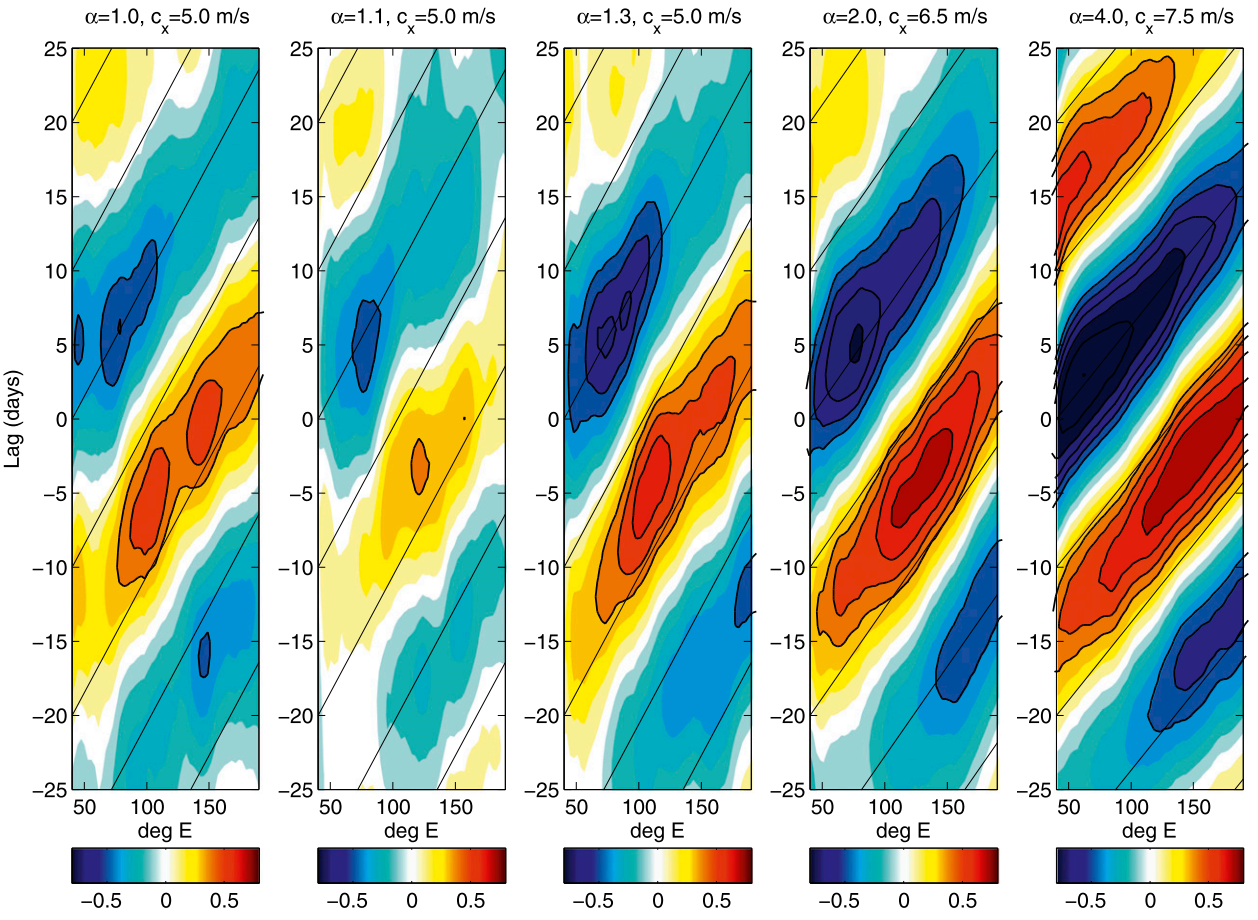

FIG. 7. As in Fig. 6, but including a quantitative estimate of the MJO speedup at positive α. Only the lag correlation coefficients of low-level winds are shown, with magnitudes greater than or equal to 0.4 contoured at an interval of 0.1. Estimated phase speed lines are superimposed for values indicated above each panel, showing the MJO wind anomalies speed up from 5 to 7.5 m s^{-1} as α is increased from 1 to 4.

We explicitly diagnose F_α as the difference in the dynamical core–predicted humidity tendency that results from using the perturbed velocity $\widetilde{\mathbf{U}}_h$ [Eq. (3)] instead of the actual velocity in the model's semi-Lagrangian moisture advection calculations. The total-column advective tendencies of s and q on the left-hand side of Eqs. (4) and (5) are likewise tracked explicitly in the model by diagnosing the total tendency due to the dynamical core (minus F_α for q).

As in Andersen and Kuang (2012), to visualize MJO fluctuations in the column MSE anomalies, a high-cloud-centric local MJO index is defined as the negative 20–100-day-filtered OLR anomaly; in our case this index is averaged horizontally from 10°S to 10°N and from 80° to 90°E. Unfiltered anomalies of 10°S–10°N column MSE and its tendency are then linearly regressed against the MJO index, lagged in longitude and time, to appraise the column energetics of hypothesized moisture-mode dynamics.

Reassuring near-monotonic sensitivities to α are evident in the corresponding regression slopes of column MSE and tendency anomalies shown in Figs. 8 and 9. As α is increased from unity, the positive MSE anomaly ahead of the MJO high-cloud core becomes higher in amplitude and the sense of eastward MSE propagation from day −6 to day 0 is clearer (Fig. 8). In the budget tendencies due to advection and F_α (Fig. 9), there is a systematic increase in the column MSE advective source ahead of the MJO moist core (Fig. 9a) as well as in the advective sink behind it (Fig. 9c). These sensitivities of the total MSE tendency are in turn primarily due to F_α, the effect of α on the column MSE budget (Figs. 9b,d), consistent with enhanced eastward propagation by horizontal MSE advection as α is increased. Some of the increase in the adiabatic component of MSE tendency is also likely due to the amplification of wind anomalies relative to OLR anomalies, particularly in the advective drying response behind the moist core (Figs. 9c,d).

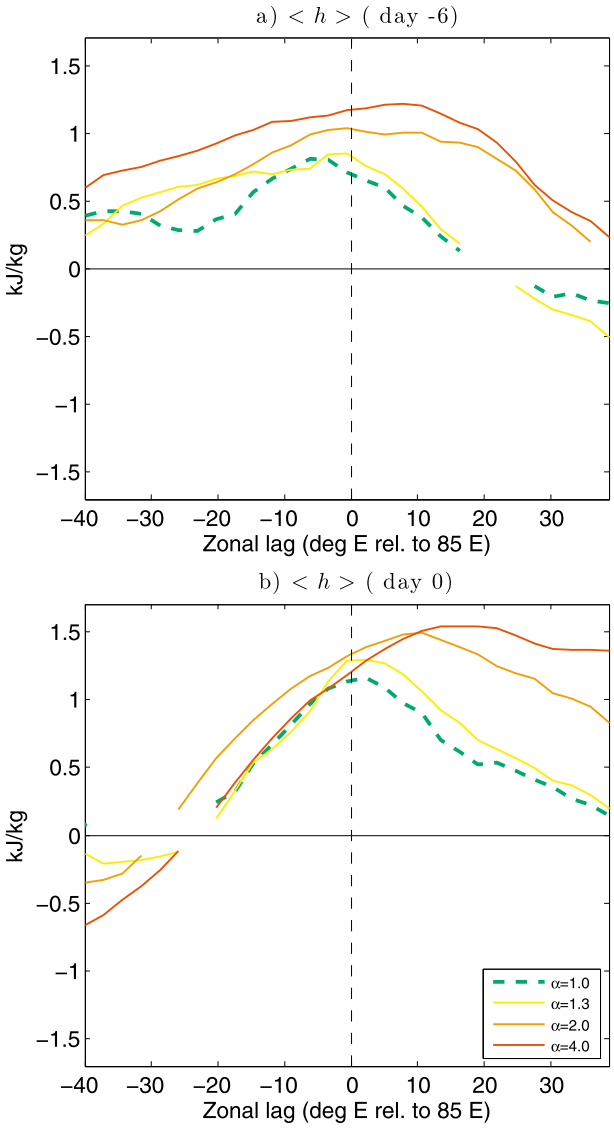

FIG. 8. Composite anomaly for 10°S–10°N column moist static energy $\langle h \rangle'$ for a $-40\,\mathrm{W\,m^{-2}}$ OLR anomaly, determined by lag regression against 20–100-day OLR averaged over 10°S–10°N, 80°–90°E for (a) $\langle h \rangle'$ leading OLR′ by 6 days and (b) at zero time lag. Only regression slopes significant at the 95% level are shown.

Overall, the results in Figs. 8 and 9 tend to suggest that α is interfering with the propagating component of the MJO as intended.

In summary, SPCAM's MJO systematically amplifies, gains coherence, and speeds up (decays and disappears) as a result of artificially increasing (decreasing) moisture advection associated with tropical vorticity anomalies.

b. Basic-state sensitivity

The above analysis has shown a strikingly monotonic sensitivity of the superparameterized MJO wind amplitude and overall phase speed to variations in the rate of moisture advection induced by tropical vorticity anomalies. It is important to verify that this is not simply the result of shifting background conditions resulting from α. Figures 10–13 (Figs. 14–15) examine SPCAM's time-mean thermodynamic (dynamic) response to varying moisture advection via α.

Increasing the amount of moisture advection induced by tropical vorticity anomalies depletes the tropics of MSE while enriching the extratropics, as shown in Fig. 10. This is an expected result since mixing of moist static energy out of the tropical reservoir is partly mediated by vorticity anomaly–induced moisture advection. Hence, increasing α amplifies the mean poleward transport of column MSE, reducing the meridional MSE gradient. This planetary response has been mitigated—but not eliminated—by restricting α's effect to the equatorial region [Eq. (3)].

Figure 11 examines the zonal structure of the mean column MSE response to α in the tropics. The Indian Ocean and eastern Pacific regions are anomalously sensitive to variations of α, losing mean column MSE as α is increased from unity more than surrounding areas, and vice versa. Consistent with a loss of tropical MSE, Fig. 13 shows that most regions in the tropics dry out and become less rainy as α is increased, and vice versa. There is an interesting flattening of the mean zonal humidity gradient and suggestive shift in the Walker circulation at high α (see section 5).

Dynamically, the planetary mean circulation responds significantly to α. Figure 14 shows that increasing the amount of moisture advection due to tropical vorticity anomalies causes a poleward shift of the midlatitude jets and decelerated upper-level flow. As α is decreased from unity, the reverse is true. Interestingly, upper-level equatorial superrotation decreases as α is increased from unity. This is opposite to the covariation of MJO amplitude and upper-level superrotation seen recently in aquaplanet sea surface temperature warming by Arnold et al. (2013).

Figure 15 shows that in the tropics the low-level wind response to increasing α from unity supports faster eastward-traveling moisture-mode disturbances over the Maritime Continent (enhanced westerlies) but resists them over the central and eastern Pacific Ocean (enhanced easterlies). This cannot explain the MJO speedup, which is observed to occur in both of these regions. At upper levels, the mean flow sensitivity to α is likewise zonally ambiguous (Fig. 14). Over the central and eastern Pacific, increasing α from unity is associated with enhanced upper-level mean westerlies, but east of 90°W the sensitivity is in the opposite sense.

The flattening of the background meridional MSE gradient at high α in Fig. 10 is also relevant to interpreting the MJO speedup signal. In the context of recent

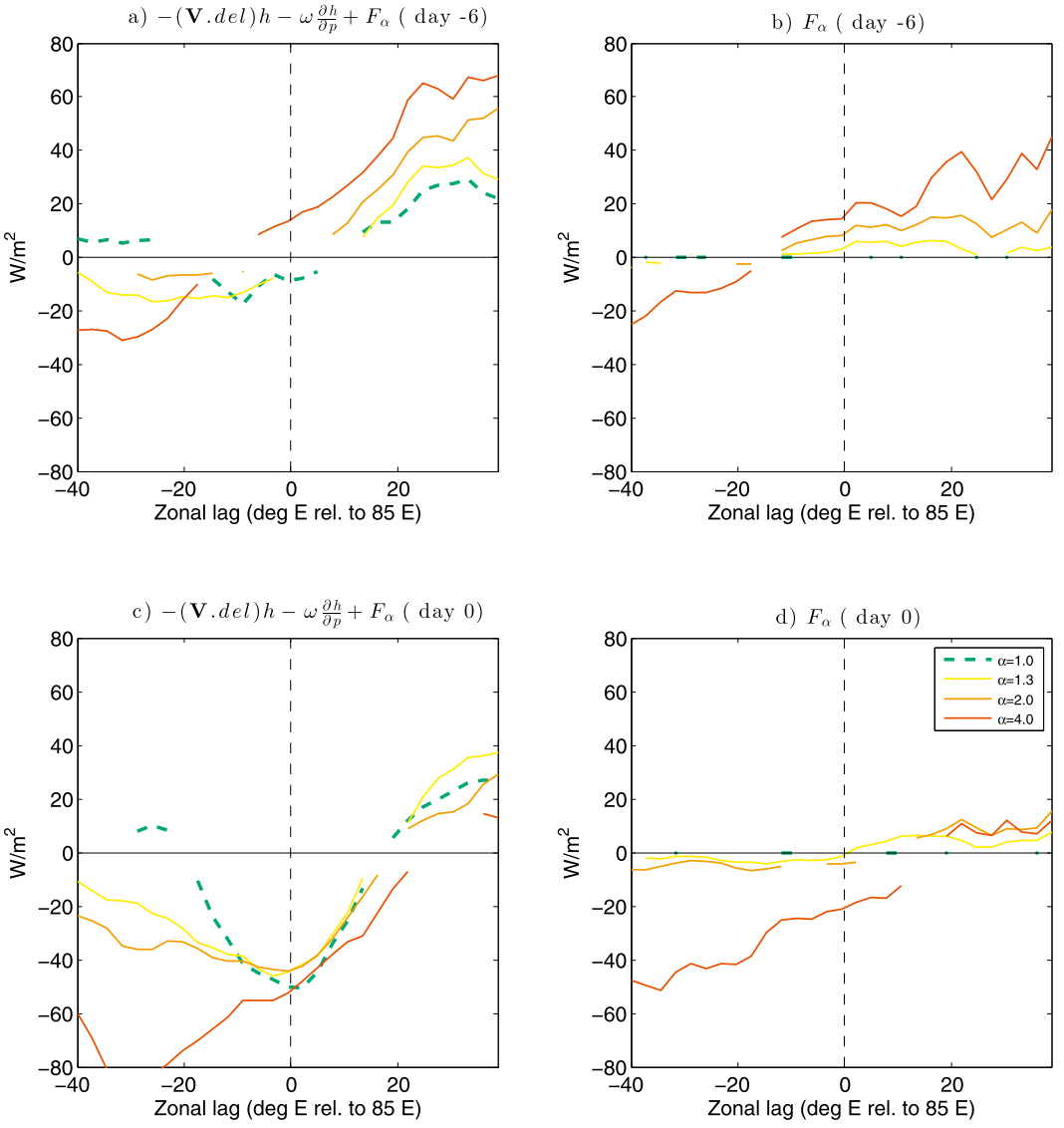

FIG. 9. As in Fig. 8, but for the MJO lag regression of (a),(c) the anomaly of total column MSE advection including the effect of α as compared to (b),(d) just the component due to α.

arguments that eddy-induced mixing promotes the MJO's eastward propagation (Maloney 2009; Andersen and Kuang 2012), decreasing the meridional MSE gradient should tend to resist a faster MJO at high α, not promote it. It is possible that buffering due to the flattening of the background meridional MSE gradient may help explain why the MJO phase speed increased only by a factor of 1.5 even with a quadrupling of α.

In summary, the interesting MJO speedup noted as α is increased from unity is unlikely to be an artifact of basic-state adjustment. Background low-level flow exhibits both westerly and easterly accelerations throughout the MJO activity region, and thus cannot explain its systematic speedup. Meanwhile, the meridional MSE gradient flattens slightly, which could be viewed to reduce background support for eastward-traveling disturbances through extratropical eddy mixing. Despite this apparent resistance from the environment, the simulated MJO speeds up.

5. Discussion

The amplification of the MJO with α is interesting since the hypothesis that horizontal moisture advection is critical to MJO propagation tends to imply a speedup response alone. One possible interpretation of the amplitude response is that the rotational component of horizontal flow anomalies excited by MJO convection

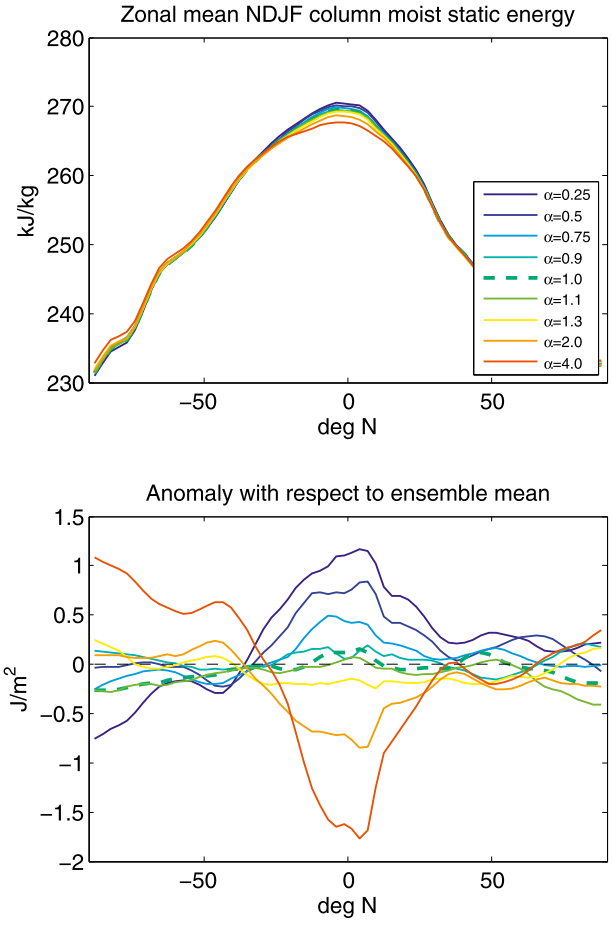

FIG. 10. (top) Time-mean column moist static energy as a function of latitude and (bottom) its anomaly with respect to the ensemble mean, showing that increasing α from unity (warm colors) depletes the tropical MSE reservoir owing to enhanced extratropical mixing and vice versa (cool colors).

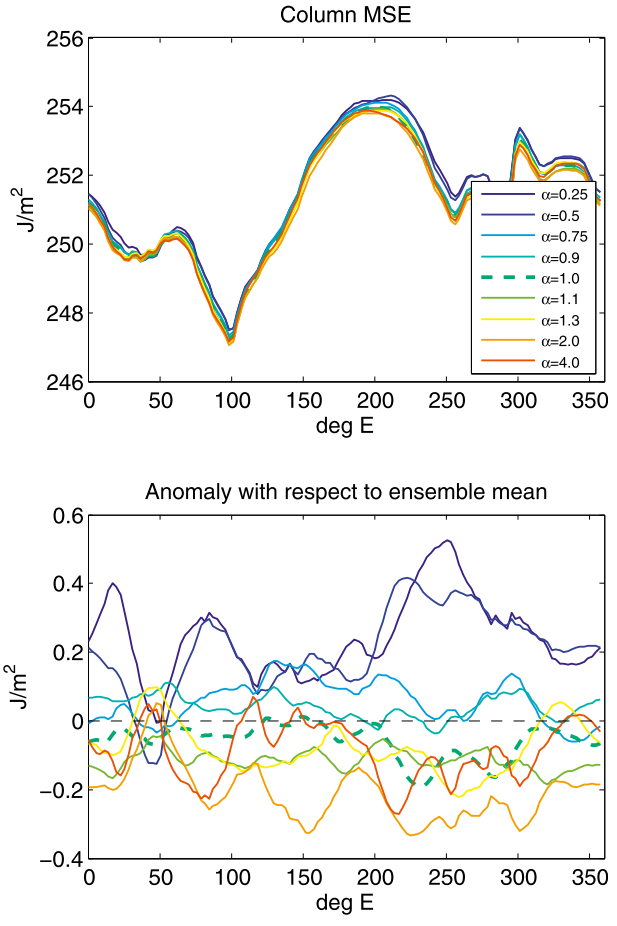

FIG. 11. (top) NDJF 10°S–10°N-mean vertically integrated moist static energy as a function of longitude and (bottom) its anomaly with respect to the ensemble mean.

also plays an important role in adiabatically maintaining the disturbance. This would be opposite to the energetic role of total horizontal moisture advection, which is known to deplete the core MSE anomaly of the MJO in this (Fig. 9) and other models (Benedict and Randall 2009; Maloney et al. 2010; Andersen and Kuang 2012) and in reanalyses (Benedict and Randall 2007).

An alternate interpretation of the MJO amplification response is that it was enabled through feedbacks impacting the basic-state gross moist stability (GMS), which is a measure of the efficiency of column MSE export as normalized by some metric of convective activity. We will follow Raymond et al. (2009) and normalize GMS by column vapor import,

$$\mathrm{GMS} = -\frac{\int \nabla\cdot(h\mathbf{v})\,dp}{\int L_v \nabla\cdot(q\mathbf{v})\,dp}, \qquad (6)$$

where h is the moist static energy and $\mathbf{v}$ is the three-dimensional velocity field.

Figure 16 examines the November–February (NDJF)-mean GMS response to α. As in other MJO-permitting global models, SPCAM's boreal winter gross moist stability is weakly positive throughout the MJO activity region in the control simulation (Fig. 16, top panel), such that moisture-mode maintenance would tend to only happen through supportive diabatic feedbacks[2] (Maloney et al. 2010; Andersen and Kuang 2012). Consistent with MJO amplification, the mean GMS decreases monotonically as α is increased from unity (Fig. 16, middle two panels). GMS reduction with MJO amplification is

[2] It could also be argued that time variations of GMS related to the MJO itself are more critical than mean-state conditions in regulating MJO amplitude in our simulations. A detailed analysis of MJO-related GMS fluctuations in the model would be necessary to further investigate this issue.

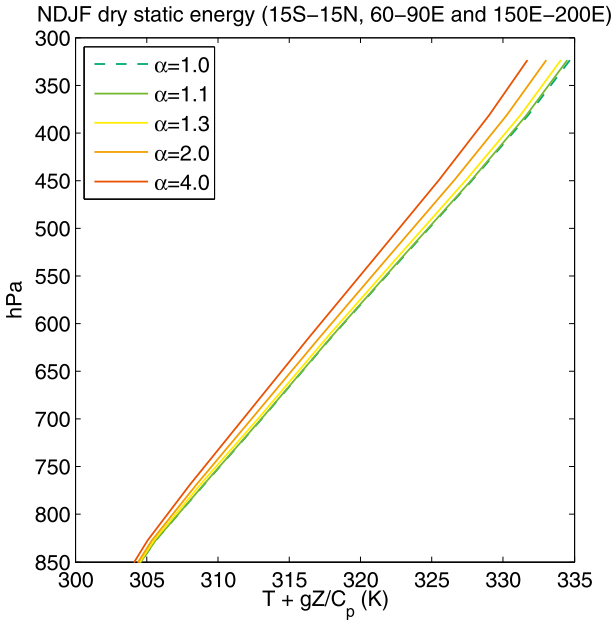

FIG. 12. NDJF 10°S–10°N-mean dry static energy averaged over the MJO activity region, showing a decrease in dry static stability as α is increased from unity.

consistent with Hannah and Maloney (2011) as well as Benedict et al. (2013, manuscript submitted to *J. Atmos. Sci.*), who recently reviewed the GMS–MJO relationship in three sets of GCMs including the SPCAM similarly configured to our control run.

It is interesting that using a convection-centric metric of MJO activity seems to tell a different story about SPCAM's MJO amplitude response to α than a wind-centric amplitude metric. Figure 3 indicates that, opposite to the wind amplitude response, intraseasonal OLR variance actually tends to decrease at high α. The question naturally arises as to how it is possible for amplified MJO wind anomalies to occur in tandem with weaker diabatic heating anomalies. One hypothesis is that environmental dry static stability decreases with α such that the mean-state arguments of Knutson and Manabe (1995) apply to SPCAM's MJO anomalies such that in a weaker stability environment the same (or in this case, smaller) diabatic heating anomaly may be balanced by a stronger vertical mass flux (hence larger horizontal wind) anomaly. However, Fig. 12 suggests that environmental dry static stability decreases far too weakly with α for this to be a primary explanation. More work is needed to understand the dichotomy between the wind and OLR amplitude responses at high α.

Although this thought experiment has focused on the MJO, it is worth noting that high-frequency tropical wave modes also speed up in response to α. Figure 17 shows that the moist Kelvin wave and tropical depression

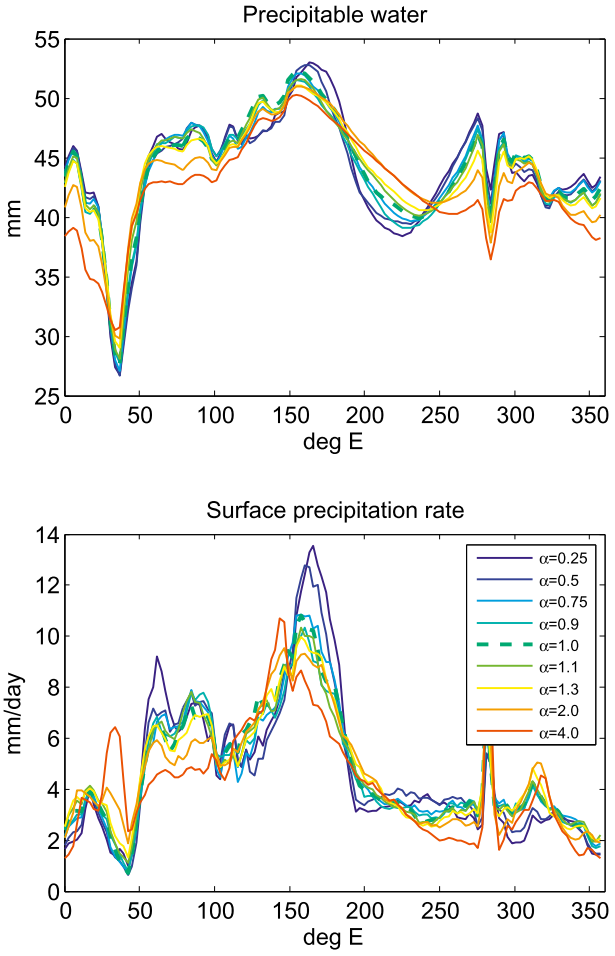

FIG. 13. NDJF 10°S–10°N-mean (top) column water vapor and (bottom) precipitation rate as a function of longitude.

wave OLR power maxima—like the MJO—amplify and shift to faster time scales for $\alpha > 1$. It is unlikely that the high-frequency response to α is an effect of a regional basic-state flow adjustment for two reasons. First, the oppositely traveling moist Kelvin waves (MKWs) and tropical depressions speed up in tandem. Second, as shown in Fig. 18, a systematic increase in the moist Kelvin wave phase speed is detectable over large zonal regions, despite regional reversals in the basic-state flow response identified there. It is plausible that the MKW speedup could have been linked to an enhancement in just the vertical component of environmental gross moist stability, relevant to the buoyancy controls on MKWs (Frierson et al. 2011). More output would be needed to investigate that hypothesis.

This relates to a general limitation of this study, which is that our simulation output was insufficient to decouple the horizontal from the vertical component of moist static energy advection. That is, only the total advective tendency from the dynamical core has been explicitly

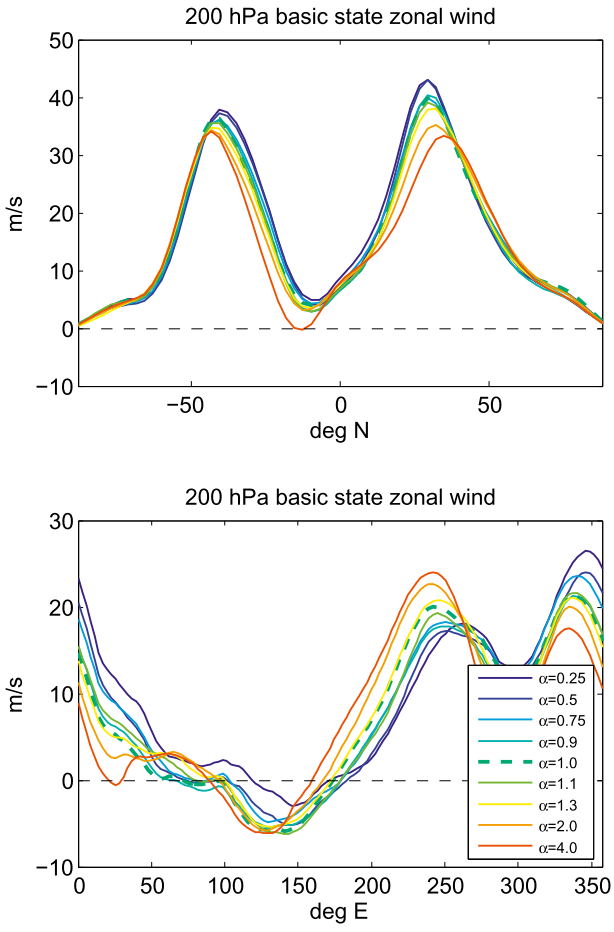

FIG. 14. Time-mean boreal winter basic-state upper-level zonal winds at 200 hPa, showing (top) meridional structure of the zonal mean and (bottom) zonal structure within 10°S–10°N.

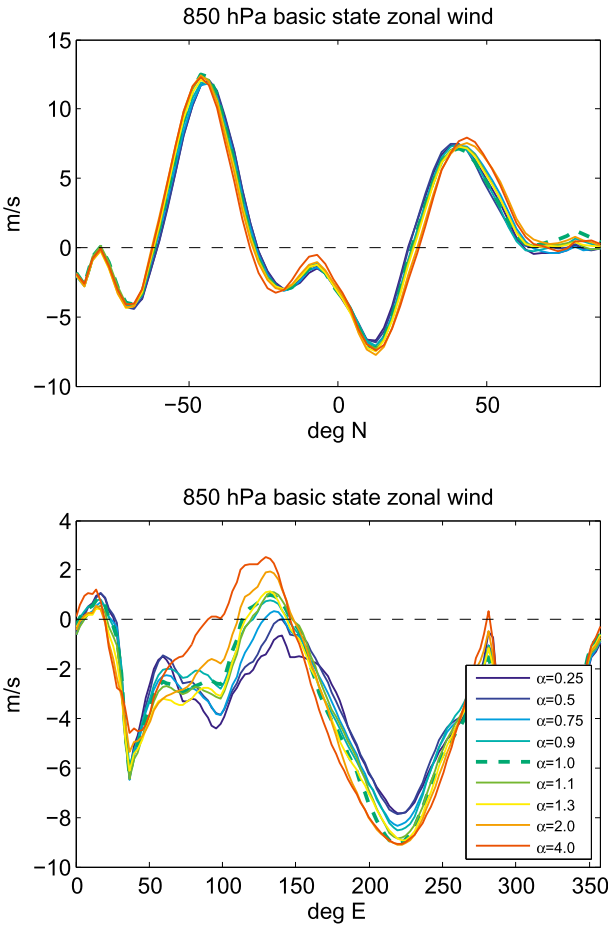

FIG. 15. As in Fig. 14, but for the lower-level flow at 850 hPa.

diagnosed and analyzed in the experiment. Furthermore, the integrations were too short to fully explore the composite vertical and horizontal structures of the MJO and its key energy balances in detail. Revisiting this experiment with enhanced output and longer integrations would thus be interesting.

This study was also limited by a strong basic-state flow response to α, which has partly obscured our analysis. This dynamical effect happened despite experiment design elements to limit time-mean effects (limiting effect of α to the tropics; avoiding artificial mass sources or sinks linked to the divergent part of the flow; maintaining the mean annual cycle of horizontal vorticity felt by moisture advection). In the future, it might be worth taking the added step of controlling zonal mean winds to verify the MJO sensitivities to α are robust to constrained tropical flow.

The mean circulation response to α is nonetheless interesting and worth some speculation. For instance, Figs. 13 and 15 suggest a drastic change in the Walker circulation, seemingly linked to a reduction in the precipitable water gradient between the eastern and western Pacific. This decreases both the warm-pool maximum and the eastern Pacific minimum, leading to a large decrease in the zonal precipitation gradient and a spreading of the maximum and minimum precipitation away from each other at high α.

It is logical to hypothesize that these changes in the mean zonal precipitable water gradient were a direct consequence of $\alpha > 1$ enhancing eddy moisture transports. To test this idea, we regress time series of the column MSE tendency due to α [F_α in Eq. (5)] against a proxy for anomalous column vapor advection by eddy zonal winds,

$$\gamma = -\widetilde{u_{850}} \frac{\partial PW}{\partial x}, \tag{7}$$

where $\widetilde{u_{850}}$ is the high-frequency (2–60 days) bandpass-filtered zonal wind anomaly at 850 hPa.

Figure 19 (left) shows that the time-mean horizontal structure of γ exhibits an expected eddy advective sink over the western warm pool and a source over the

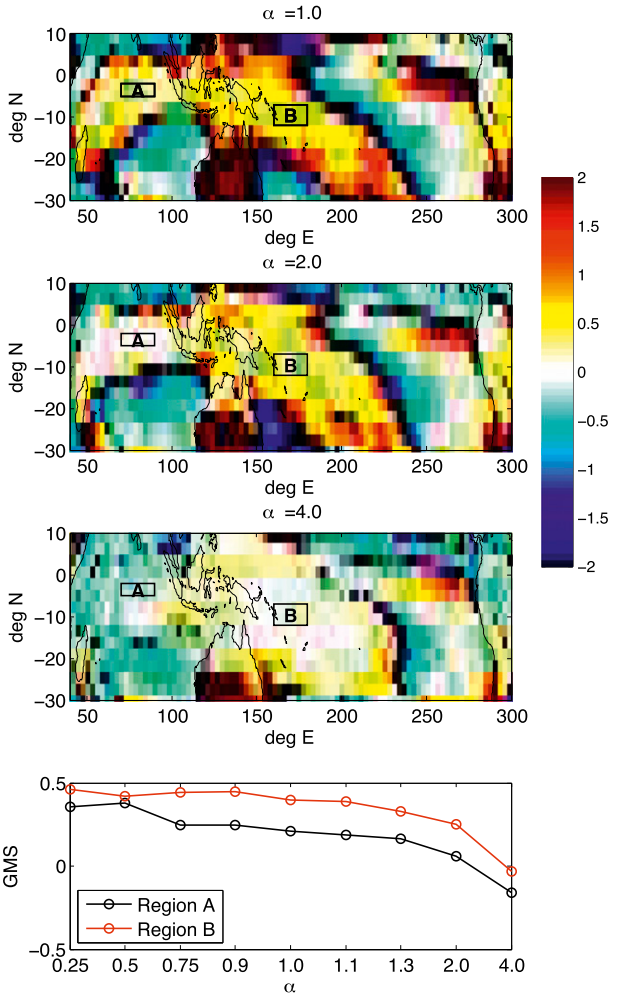

FIG. 16. Time-mean boreal winter gross moist stability [Eq. (6)] for (top) the control simulation, (second row) $\alpha = 2$, and (third row) $\alpha = 4$. (bottom) Mean GMS decreases with α for the two boxed subregions.

eastern Pacific. With higher α, although the precipitable water gradient and γ are slightly weakened, the eddy moisture flux retains a fairly similar zonal structure and shape. Since the rotational part of the eddy moisture flux is multiplied by α in calculating the total q dynamic tendency, there should be a stronger effective moisture sink in the west and source in the east for $\alpha > 1$. The robustly positive regression slopes of $\partial F_\alpha/\partial\gamma$ (Fig. 19, right) confirm that α acts to boost the baseline zonal eddy moisture flux pattern in this fashion. This clearly supports the idea that eddy fluxes are a driver of the reduced PW gradients across the Pacific at high α, and associated Walker circulation changes, though it does not exclude that other processes could also be important.

Finally, although this thought experiment has focused primarily on the adiabatic propagation of the MJO,

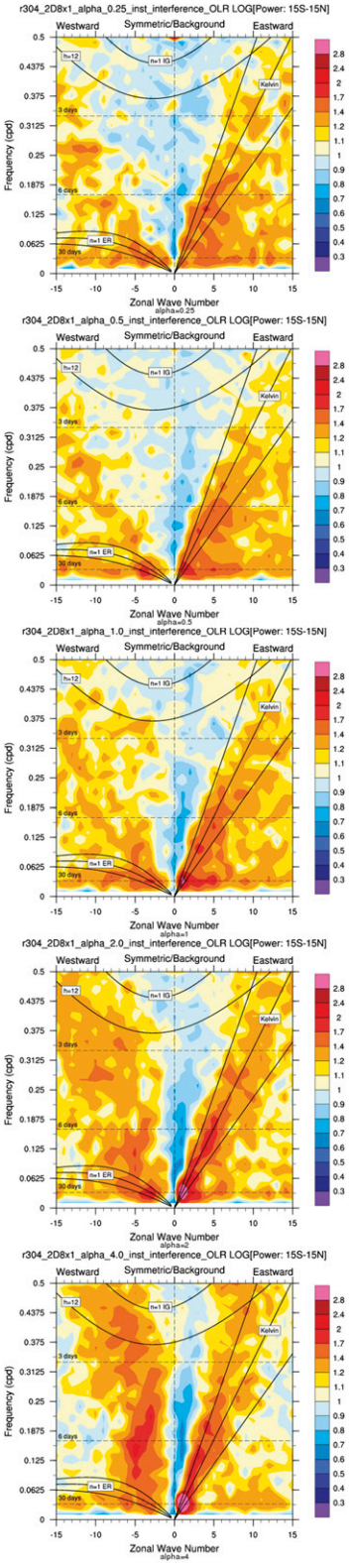

FIG. 17. Symmetric wavenumber–frequency signal-to-noise spectra for unfiltered 15°S–15°N OLR simulated for (top)–(bottom) $\alpha = 0.25$, 0.5, 1, 2, and 4.

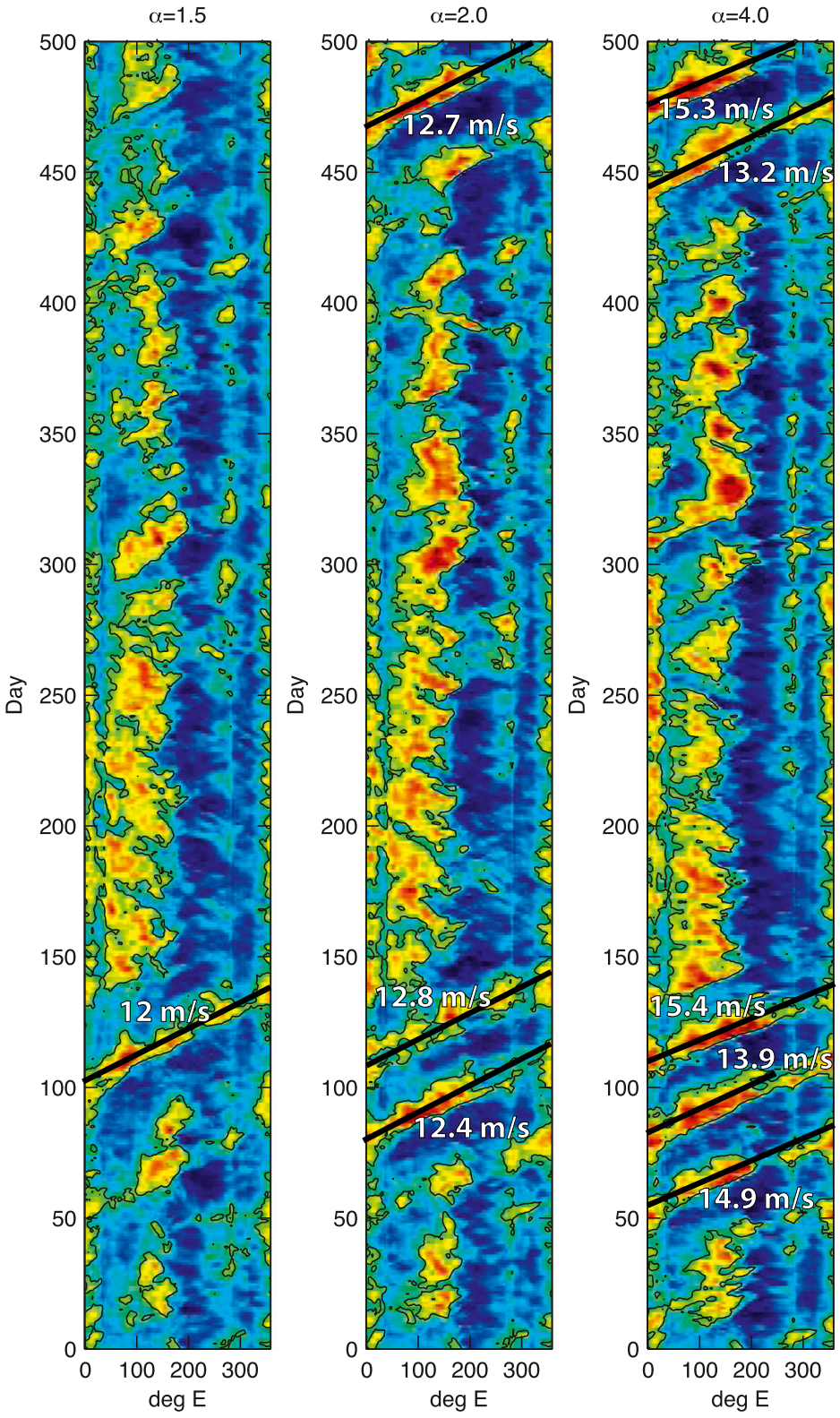

FIG. 18. Time–longitude evolution of 10°S–10°N, 850-hPa zonal wind anomalies for the 1.5 years of simulation, showing systematic increase of the moist Kelvin wave phase speed as α is increased over the range 1.5–4.

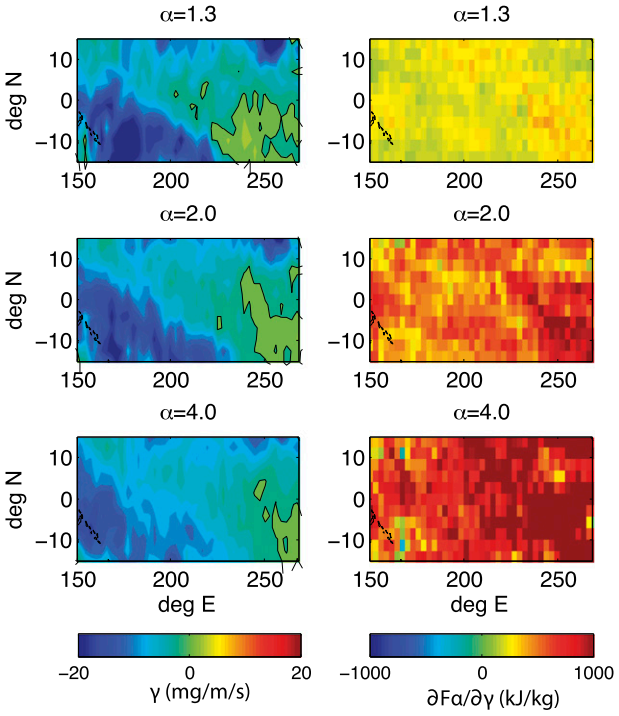

FIG. 19. (left) Time-mean maps of a proxy for moisture advection by the eddy zonal wind γ shown for (top)–(bottom) increasing α. (right) Corresponding maps of the γ-regressed MSE tendency due to α, suggesting α amplifies the baseline pattern of eddy zonal moisture advection.

future work would also be helpful to see if similarly clean monotonic and causal sensitivities can be detected for other processes critical to the diabatic maintenance of SPCAM's MJO—for instance, by longwave heating and surface evaporation. Others have shown in mechanism-denial twin experiments on idealized aquaplanets that MJO-permitting global models can disagree about the relative importance of these two processes in a weakly positive GMS environment (Maloney et al. 2010; Kiranmayi and Maloney 2011; Andersen and Kuang 2012). Real-geography SPCAM v3.0 remains an especially attractive model for this type of analysis given its especially realistic boreal winter basic state and well-validated[3] MJO. The α experiment design of hunting for monotonic sensitivities in response to a smoothly varying external control parameter may also prove to be clarifying for examining diabatic processes.

[3] However, our configuration of SPCAM3.0 that uses unusually tiny cloud resolving model (CRM) arrays has not been as thoroughly validated. It would be interesting to verify that its behavior is fully representative of the model's baseline behavior using the more typical multiscale modeling configuration with large CRMs.

6. Conclusions

From the moisture-mode paradigm, the MJO may be viewed as the result of an intrinsic predisposition for tropical deep convection to self-aggregate on large scales through internal feedbacks (Bretherton et al. 2005; Muller and Held 2012). Coupled to horizontal advection, this mechanism can manifest as a slow eastward-traveling disturbance.

In this study, we have tested causally whether the rotational component of horizontal moisture advection is critical to the realistic MJO signal in the Superparameterized Community Atmosphere Model (SPCAM), version 3.0 using a new method. A control parameter α was introduced to isolate the MJO response to artificially decreasing ($\alpha < 1$) versus increasing ($\alpha > 1$) the rate of horizontal moisture advection associated with vorticity anomalies in the tropics. The influence of α was applied inline during free-running simulations and its effect diagnosed from statistical analysis of the resulting boreal winter MJO signal.

SPCAM's clean MJO response to α strongly affirms the moisture-mode view that horizontal moisture advection is critical to MJO dynamics. When tropical moisture advection is artificially enhanced, SPCAM's MJO amplifies, speeds up, and circumnavigates more of the globe. When tropical moisture advection is reduced, SPCAM's MJO shuts down. This speedup response is nearly monotonic to α and happens despite a basic-state sensitivity that resists or buffers it. The test thus provides causal affirmation of an existing body of evidence from this and other modern MJO-permitting global climate models that exhibit diagnostic energy budget signatures suggestively consistent with the idea that horizontal moisture advection plays a critical role in MJO propagation. The test especially emphasizes the importance of the rotational flow component, and complements recent idealized studies by showing that sensitivities linked to it are clear even in the fully nonlinear world of SPCAM with a realistic basic state and real geography.

In all, the results affirm the idea of an MJO that moves east because of horizontal moisture advection, perhaps slowed by the existence of rotational memory carried by moisture anomalies embedded in the tropical vorticity field.

Acknowledgments. This work was funded by the National Oceanographic and Atmospheric Administration's Climate and Global Change Postdoctoral Fellowship Program. CB acknowledges additional support from the National Science Foundation (NSF) Center for Multiscale Modeling of Atmospheric Processes (CMMAP; Grant ATM0425247). This work used the Extreme Science and Engineering Discovery Environment (XSEDE),

which is supported by NSF Grant OCI-1053575. Thanks to Tom Ackerman, Zhiming Kuang, Dargan Frierson, Peter Blossey, Roj Marchand, and Dale Durran for feedback that was critical to this work. Special thanks to Eric Maloney and an anonymous reviewer for great feedback that helped improve an earlier draft of this manuscript and to Marat Khairoutdinov for developing, tuning, and distributing SPCAM3.0 through CMMAP.

REFERENCES

Anderson, J. A., 2012: Investigations of the convectively coupled equatorial waves and the Madden–Julian oscillation. Ph.D. dissertation, Harvard University, 290 pp.

——, and Z. Kuang, 2012: Moist static energy budget of MJO-like disturbances in the atmosphere of a zonally symmetric aquaplanet. *J. Climate,* **25,** 2782–2804.

Arnold, N. P., Z. Kuang, and E. Tziperman, 2013: Enhanced MJO-like variability at high SST. *J. Climate,* **26,** 988–1001.

Benedict, J. J., and D. A. Randall, 2007: Observed characteristics of the MJO relative to maximum rainfall. *J. Atmos. Sci.,* **64,** 2332–2354.

——, and ——, 2009: Structure of the Madden–Julian oscillation in the superparameterized CAM. *J. Atmos. Sci.,* **66,** 3277–3296.

——, and ——, 2011: Impacts of idealized air–sea coupling on Madden–Julian oscillation structure in the superparameterized CAM. *J. Atmos. Sci.,* **68,** 1990–2008.

Bretherton, C. S., P. N. Blossey, and M. Khairoutdinov, 2005: An energy-balance analysis of deep convective self-aggregation above uniform SST. *J. Atmos. Sci.,* **62,** 4273–4292.

Chikira, M., 2014: Eastward-propagating intraseasonal oscillation represented by Chikira–Sugiyama cumulus parameterization. Part II: Understanding moisture variation under weak temperature gradient balance. *J. Atmos. Sci.,* **71,** 615–639.

——, and M. Sugiyama, 2013: Eastward-propagating intraseasonal oscillation represented by Chikira–Sugiyama cumulus parameterization. Part I: Comparison with observation and reanalysis. *J. Atmos. Sci.,* **70,** 3920–3939.

Collins, W. D., and P. J. Rasch, 2004: Description of the NCAR Community Atmosphere Model (CAM 3.0). NCAR Tech. Note NCAR/TN-464+STR, 214 pp.

Frierson, D. M., D. Kim, I.-S. Kang, M. I. Lee, and J.-L. Lin, 2011: Structure of AGCM-simulated convectively coupled equatorial waves and sensitivity to convective parameterization. *J. Atmos. Sci.,* **68,** 26–45.

Fuchs, Ž., and D. J. Raymond, 2002: Large-scale modes of a nonrotating atmosphere with water vapor and cloud–radiation feedbacks. *J. Atmos. Sci.,* **59,** 1669–1679.

——, and ——, 2005: Large-scale modes in a rotating atmosphere with radiative–convective instability and WISHE. *J. Atmos. Sci.,* **62,** 4084–4094.

Hannah, W. M., and E. D. Maloney, 2011: The role of moisture–convection feedbacks in simulating the Madden–Julian oscillation. *J. Climate,* **24,** 2754–2770.

Hirons, L. C., P. Inness, F. Vitart, and P. Bechtold, 2013: Understanding advances in the simulation of intraseasonal variability in the ECMWF model. Part I: The representation of the MJO. *Quart. J. Roy. Meteor. Soc.,* **139,** 1417–1426.

Khairoutdinov, M. F., and D. A. Randall, 2003: Cloud resolving modeling of the ARM summer 1997 IOP: Model formulation, results, uncertainties, and sensitivities. *J. Atmos. Sci.,* **60,** 607–625.

——, ——, and C. DeMott, 2005: Simulations of the atmospheric general circulation using a cloud-resolving model as a superparameterization of physical processes. *J. Atmos. Sci.,* **62,** 2136–2154.

——, C. DeMott, and D. A. Randall, 2008: Evaluation of the simulated interannual and subseasonal variability in an AMIP-style simulation using the CSU multi-scale modeling framework. *J. Climate,* **21,** 413–431.

Kim, D., and Coauthors, 2009: Application of MJO simulation diagnostics to climate models. *J. Climate,* **22,** 6413–6436.

Kiranmayi, L., and E. D. Maloney, 2011: Intraseasonal moist static energy budget in reanalysis data. *J. Geophys. Res.,* **116,** D21117, doi:10.1029/2011JD016031.

Knutson, T. R., and S. Manabe, 1995: Time-mean response over the tropical Pacific to increased CO_2 in a coupled ocean–atmosphere model. *J. Climate,* **8,** 2181–2199.

Maloney, E. D., 2009: The moist static energy budget of a composite tropical intraseasonal oscillation in a climate model. *J. Climate,* **22,** 711–729.

——, A. H. Sobel, and W. M. Hannah, 2010: Intraseasonal variability in an aquaplanet general circulation model. *J. Adv. Model. Earth Syst.,* **2** (5), doi:10.3894/JAMES.2010.2.5.

Muller, C. J., and I. M. Held, 2012: Detailed investigation of the self-aggregation of convection in cloud-resolving simulations. *J. Atmos. Sci.,* **69,** 2551–2565.

Randall, D., M. Khairoutdinov, A. Arakawa, and W. Grabowski, 2003: Breaking the cloud parameterization deadlock. *Bull. Amer. Meteor. Soc.,* **84,** 1547–1562.

Raymond, D. J., and Ž. Fuchs, 2009: Moisture modes and the Madden–Julian oscillation. *J. Climate,* **22,** 3031–3046.

——, S. Sessions, A. H. Sobel, and Z. Fuchs, 2009: The mechanics of gross moist stability. *J. Adv. Model. Earth Syst.,* **1** (9), doi:10.3894/JAMES.2009.1.9.

Sobel, A., and E. Maloney, 2012: An idealized semi-empirical framework for modeling the Madden–Julian oscillation. *J. Atmos. Sci.,* **69,** 1691–1703.

——, and ——, 2013: Moisture modes and the eastward propagation of the MJO. *J. Atmos. Sci.,* **70,** 187–192.

——, J. Nilsson, and L. M. Polvani, 2001: The weak temperature gradient approximation and balanced tropical moisture waves. *J. Atmos. Sci.,* **58,** 3650–3665.

Stan, C., M. Khairoutdinov, C. A. DeMott, V. Krishnamurthy, D. M. Straus, D. A. Randall, J. L. Kinter, and J. Shukla, 2010: An ocean-atmosphere climate simulation with an embedded cloud resolving model. *Geophys. Res. Lett.,* **37,** L01702, doi:10.1029/2009GL040822.

Sugiyama, M., 2009a: The moisture mode in the quasi-equilibrium tropical circulation model. Part I: Analysis based on the weak temperature gradient approximation. *J. Atmos. Sci.,* **66,** 1507–1523.

——, 2009b: The moisture mode in the quasi-equilibrium tropical circulation model. Part II: Nonlinear behavior on an equatorial β plane. *J. Atmos. Sci.,* **66,** 1525–1542.

Thayer-Calder, K., and D. A. Randall, 2009: The role of convective moistening in the Madden–Julian oscillation. *J. Atmos. Sci.,* **66,** 3297–3312.

Wheeler, M. C., and H. H. Hendon, 2004: An all-season real-time multivariate MJO index: Development of an index for monitoring and prediction. *Mon. Wea. Rev.,* **132,** 1917–1932.

Yu, J.-Y., and J. D. Neelin, 1994: Modes of tropical variability under convective adjustment and the Madden–Julian oscillation. Part II: Numerical results. *J. Atmos. Sci.,* **51,** 1895–1914.